IEEE Access
Multidisciplinary | Rapid Review | Open Access Journal

Received 14 March 2023, accepted 10 April 2023, date of publication 12 April 2023, date of current version 20 April 2023.

Digital Object Identifier 10.1109/ACCESS.2023.3266646

RESEARCH ARTICLE

Series Resonant Converter With Multiple Resonant Points Using Sequential PWM for Electrical Vehicle On-Board Charger

JONG-WOO KIM, (Member, IEEE), DOHONG LEE, (Student Member, IEEE), AND YOUNGHOON CHO, (Senior Member, IEEE)

Deportment of Electronics and Electrical Engineering, Konkuk University, Gwangjin-Gu, Seoul 05028, South Korea

Corresponding author: Jong-Woo Kim (jongwookim@konkuk.ac.kr)

This work was supported by Konkuk University, in 2023.

ABSTRACT In electric vehicle (EV) charging applications, maintaining high efficiency over a wide output voltage range is considered the most challenging mission. Pulse width modulation (PWM) controlled resonant converter can be a nice candidate, because its output voltage boosting capability is independent to the resonant tank components. However, it reveals its limitation showing efficiency drop between two resonant points. This paper proposes a resonant converter with ''sequential PWM'' achieving multiple resonant points while doubling the output voltage. The proposed converter significantly reduces turnoff loss and maximum resonant current by having multiple resonant points while doubling the output voltage. Accordingly, proposed converter maintains competitive high efficiency over a wide output voltage range.

INDEX TERMS EV charger, resonant converter, wide voltage range.

I. INTRODUCTION

Resonant converter is a mainstream among various DC-DC converter topologies due to its superior performance and cost effectiveness [1], [2], [3], [4], [5], [6], [7], [8], [9], [10], [19]. In electrical vehicle (EV) charging applications, resonant converter needs to cover wide output voltage range according to the battery charging curve presented in Fig. 1. EV battery charging can be divided into 3 regions according to the battery voltage: constant voltage (CV), constant power (CP), and constant current (CC) regions. Out of three operating regions, achieving highest efficiency in CP region is critical due to following reasons: 1. CP region has the highest power consumption. 2. Users mostly manage the battery voltage level in CP region to maintain sufficient driving distance.

Fig. 2(a) presents an LLC resonant converter. LLC converter is the most popular resonant converter in EV chargers due to a simple structure and inherent zero voltage switching. The resonant frequency (FR) of LLC converter is determined by the resonant inductor (LR) and capacitor (CR). LLC converter is usually controlled by pulse frequency modulation (PFM) in order to adjust the voltage conversion ratio. When the switching frequency (FS) is equal to the resonant frequency, the voltage conversion ratio of LLC converter becomes the turns ratio of the transformer. When a smaller

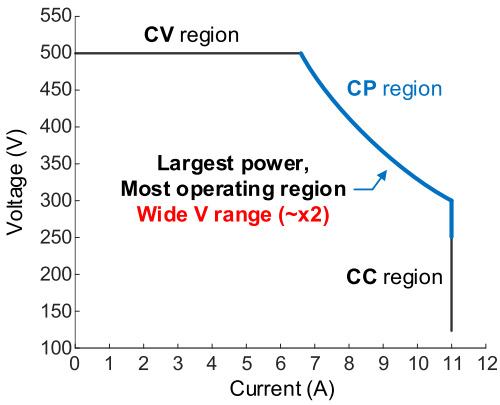

FIGURE 1. V-I curve of EV on-board charger with 3.3 kW/11 A output.

The associate editor coordinating the review of this manuscript and approving it for publication was Sonia F. Pinto.

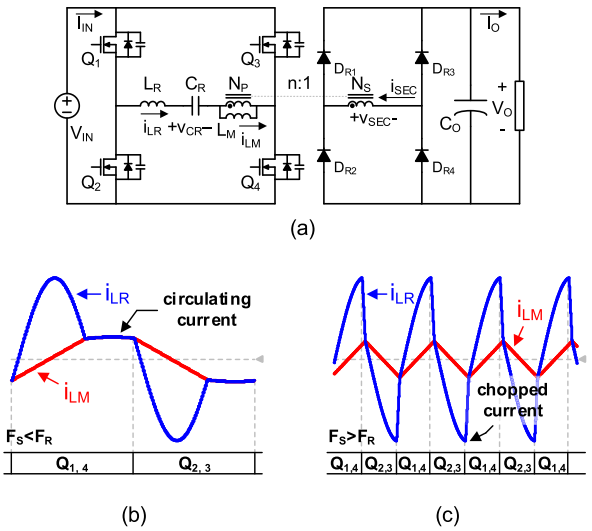

FIGURE 2. (a) An LLC resonant converter, (b) resonant current waveform when $F_S > F_R$, and (c) when $F_S < F_R$.

output voltage is required, the switching frequency becomes larger than the resonant frequency as shown in Fig. 2(b), in order to chop the resonant current delivered to the output side. On the other hand, when a higher output voltage is required, the switching frequency becomes smaller than the resonant frequency as shown in Fig. 2(c). This is in order to accumulate circulating current in the resonant capacitor. Accumulated charges are delivered to the output side during the next switching period. In a boosting region, the peak value of the resonant current becomes large, causing a larger maximum flux density in the resonant inductor. Also, the circulating current needs to be large enough when a high output voltage conversion ratio is required, causing a larger flux density in the transformer core. Therefore, LLC converter with PFM suffers from large magnetic component size and decreased efficiency especially designed with a high boosting voltage gain.

In order to provide a high boosting gain with LLC converter, various approaches have been investigated. Among those approaches, the most effective ways to improve boosting capability are topology morphing and pulse width modulation (PWM) techniques.

Topology morphing techniques [16], [17], [18] change the configuration of primary and/or secondary side of LLC converter. By doing so, primary side of LLC converter in Fig. 2 can be either half bridge or full bridge inverter. Also, secondary side rectifier can be either full bridge or voltage doubler rectifier. By doing so, the voltage conversion ratio can be wider than 4 times easily. However, most of topology morphing techniques depend on PFM to cover the gain between morphed topologies. In this case, the limitation of LLC converter still remains because PFM still needs to cover two times of gain.

PWM techniques adapted duty ratio control to make LLC converter as an isolated boost [8], [9], [10], [11], [12], [13], [14], [15] or buck [19], [20], [21], [22], [23] converter. By doing so, LLC converter reduces dependency on the circulating current to obtain a wide gain range, minimizing the circulating current in the resonant components design. However, it suffers from a large peak of the resonant current and turnoff losses.

In order to overcome the limitations of the state-of-the-art technologies, PWM morphing technology was proposed in [10]. PWM morphing technology gradually increases the duty cycle of secondary rectifier as higher output voltage is needed. When it operates with full bridge rectifier, the duty cycle of a rectifier switch is 0.5. When the output voltage increases, the duty cycle increases. When the output voltage is doubled, the duty ratio naturally increases to 1, forming a voltage doubler rectifier at the secondary side. This method can achieve high boosting gain without relying on circulating current. Furthermore, it naturally achieves sinusoidal resonant current waveform with doubled output voltage. However, it still has large peak current in a boosting region, causing large resonant inductor and turnoff loss. Based on the review of state-of-the-art technologies, we can recognize unresolved missions in DC-DC converter for EV charger as follows:

1) Both PFM and PWM control suffer from increased size of magnetic components. PFM requires larger magnetic components for enough circulating current, and PWM requires a larger resonant inductor for smaller peak current and turnoff losses.

2) Peak efficiency occurs only when the voltage conversion ratio is the turns ratio times the powers of 2 ($n \cdot 2^k$). Considering that the output voltage varies by around or less than 2 times in CP region, the efficiency profile is not optimal for on-board charging applications.

This paper proposes a new PWM controlled resonant converter achieving 'multiple resonant points' while doubling the output voltage. The proposed converter utilizes series input parallel output transformers, and applies PWM control to each transformer in a sequence. By doing so, the proposed converter can decrease both the maximum resonant current and turnoff loss in a PWM resonant converter.

II. PROPOSED CONVERTER

Fig. 3 presents proposed PWM resonant converter. Two transformers TR_1 and TR_2 are adapted. Secondary side windings of transformers are connected in parallel, in order to reduce current stress of each transformer. Primary side windings of transformers are connected in series so that the resonant currents are equally shared in two transformers.

Nowadays, EV chargers try to improve maximum power capability. So, series input parallel output (SIPO) structure is an appropriate structure, achieving both less current stress and balanced current. The number of turns of a transformer is N_{P1} and N_{P2} at the primary side and N_{S1} and N_{S2} at the secondary side. n is the effective turns ratio of the proposed converter, which will be discussed in detail later. The resonant tank components are L_R and C_R in series. Assuming the

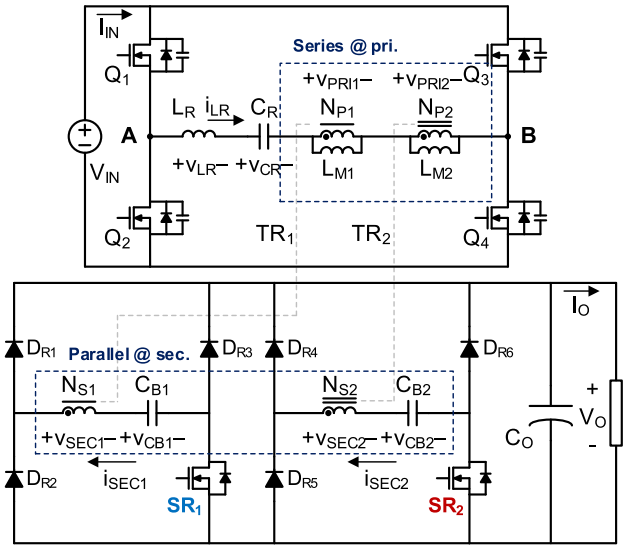

FIGURE 3. Proposed converter.

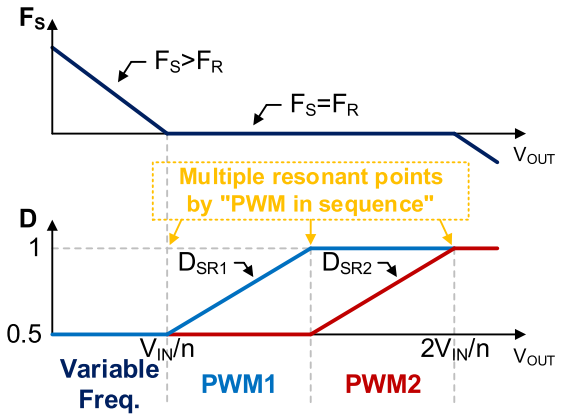

FIGURE 4. 'Sequential PWM' control concept of the proposed converter.

magnetizing inductors of the transformers are much larger than L_R, the proposed converter can be considered a series resonant converter. Blocking capacitors C_{B1} and C_{B2} are implemented in series with the secondary side windings of transformers.

Fig. 4 presents control concept of the proposed converter. When the output voltage V_{OUT} is smaller than V_{IN}/n, the proposed converter is controlled by the switching frequency F_S. When the gain increases, F_S increases but smaller than the resonant frequency $F_R(=1/2\pi\sqrt{L_RC_R})$. When V_{OUT} becomes V_{IN}/n, F_S becomes F_R and the proposed converter has a sinusoidal resonant current waveform. Here, the proposed converter achieves the first resonant point. When V_{OUT} becomes higher than V_{IN}/n, F_S is still F_R but duty cycles of the synchronous rectifier switches (D_{SR1} and D_{SR2}) increase in a sequence. First, D_{SR1} increases from 0.5 to 1 as V_{OUT} increases. When D_{SR1} reaches 1, the proposed converter achieves the second resonant point. If V_{OUT} further increases,

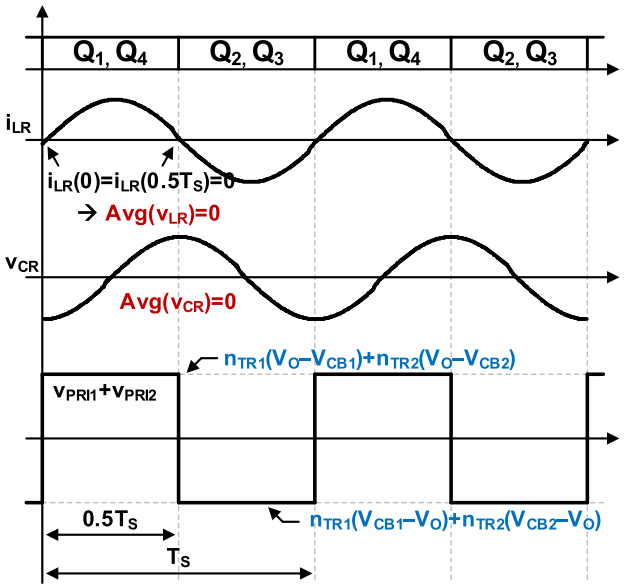

FIGURE 5. Primary side waveforms of the proposed converter at a resonant point.

now D_{SR2} increases from 0.5 to 1. When D_{SR2} reaches 1, the proposed converter achieves the third resonant point. V_{OUT} becomes $2V_{IN}/n$ because the secondary side rectifier becomes a pure voltage doubler. It can be noted that the proposed converter achieves "multiple resonant points" with sequential PWM control and SIPO structure.

III. OPERATION OF THE PROPOSED CONVERTER

A. OPERATION AT THREE RESONANT POINTS

Fig. 5 presents primary side waveforms of the proposed converter at a resonant point. F_S is F_R. Resonant current waveform i_{LR} is sinusoidal. The total transformer voltage at the primary side can be presented as follows:

$$v_{PRI1} + v_{PRI2} = n_{TR1}v_{SEC1} + n_{TR2}v_{SEC2}, \quad (1)$$

where v_{PRI1}, v_{PRI2}, v_{SEC1}, v_{SEC2}, n_{TR1}, and n_{TR2} present primary side voltage, secondary side voltage, and turns ratio (N_{P1}/N_{S1}, N_{P2}/N_{S2}) of transformer 1 and 2.

From $t = 0$ to $0.5T_S$, Q_1 and Q_4 are turned on. Applying KVL at the primary side of the proposed converter leads to the following equation:

$$V_{IN} = v_{LR} + v_{CR} + v_{PRI1} + v_{PRI2}. \quad (2)$$

Substituting (1) into (2) leads to the following equation:

$$V_{IN} = v_{LR} + v_{CR} + n_{TR1}v_{SEC1} + n_{TR2}v_{SEC2}. \quad (3)$$

In Fig. 5, $i_{LR}(0) = i_{LR}(0.5T_S) = 0$. Therefore, the average voltage across L_R during $t = 0{\sim}0.5T_S$ becomes zero:

$$< v_{LR} >_{0.5T_S} = 0. \quad (4)$$

At a resonant point, v_{CR} is sinusoidal and its average value is also zero:

$$< v_{CR} >_{0.5T_S} = 0. \quad (5)$$

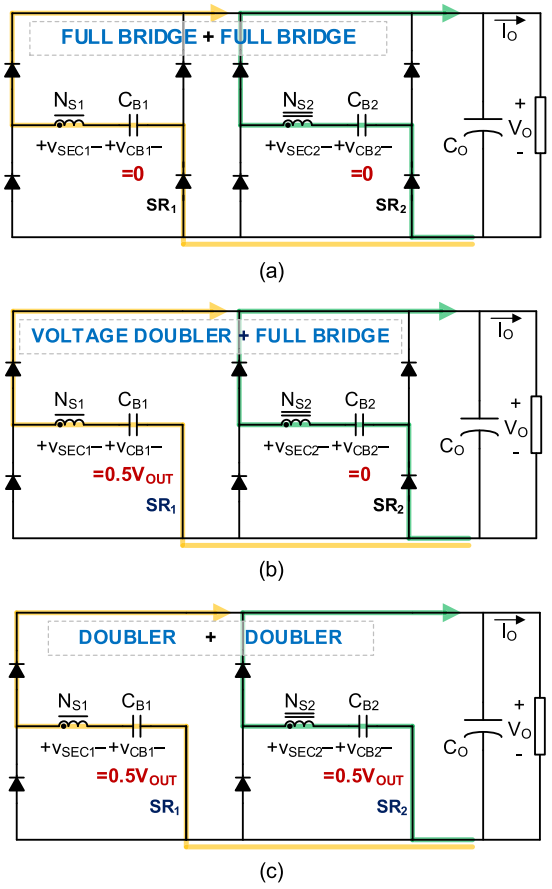

FIGURE 6. Formation of the secondary side rectifier and current paths when $i_{LR} > 0$ at the (a) first resonant point ($D_{SR1} = D_{SR2} = 0.5$), (b) second resonant point ($D_{SR1} = 1$, $D_{SR2} = 0.5$), and (c) third resonant point ($D_{SR1} = D_{SR2} = 1$).

Averaging (3) during t = 0∼0.5T_S leads to the following equation:

$$V_{IN} = n_{TR1} < v_{SEC1} >_{0.5T_S} + n_{TR2} < v_{SEC2} >_{0.5T_S}, \quad (6)$$

$$V_{IN} = n_{TR1}(V_O - V_{CB1}) + n_{TR2}(V_O - V_{CB2}). \quad (7)$$

Based on (7), the voltage conversion ratio of the proposed converter at three resonant points can be obtained in the following paragraphs.

1) THE FIRST RESONANT POINT ($D_{SR1} = D_{SR2} = 0.5$)

Fig. 6(a) presents secondary side rectifier of the proposed converter at the first resonant point. Two full bridge rectifiers are connected in parallel, as all semiconductor devices are operating as diodes. The average voltage across the blocking capacitors C_{B1} and C_{B2} is zero by the voltage second balance of the secondary side of the transformer:

$$V_{CB1} = V_{CB2} = 0. \quad (8)$$

Combining (7) and (8) allows us to find the output voltage of the proposed converter at the first resonant point as follows:

$$V_O = \frac{V_{IN}}{n_{TR1} + n_{TR2}}. \quad (9)$$

2) THE SECOND RESONANT POINT ($D_{SR1} = 1$, $D_{SR2} = 0.5$)

Fig. 6(b) presents secondary side rectifier of the proposed converter at the second resonant point. A full bridge and a voltage doubler rectifiers are connected in parallel because SR_1 is always turned on. The average voltages across the blocking capacitors become $V_{OUT}/2$ and zero respectively, by the voltage second balance of the secondary side of the transformers:

$$V_{CB1} = 0.5V_O, \quad (10)$$

$$V_{CB2} = 0. \quad (11)$$

Combining (7), (10), and (11) allows us to find the output voltage of the proposed converter at the second resonant point as follows:

$$V_O = \frac{V_{IN}}{0.5n_{TR1} + n_{TR2}}. \quad (12)$$

3) THE THIRD RESONANT POINT ($D_{SR1} = 1$, $D_{SR2} = 1$)

Fig. 6(c) presents secondary side rectifier of the proposed converter at the third resonant point. Two voltage doubler rectifiers are connected in parallel because both SR_1 and SR_2 are always turned on. The average voltage across the blocking capacitors becomes $V_{OUT}/2$ for both, by the voltage second balance of the secondary side of the transformers:

$$V_{CB1} = V_{CB2} = 0.5V_O. \quad (13)$$

Combining (7) and (13) allows us to find the output voltage of the proposed converter at the third resonant point as follows:

$$V_O = \frac{2V_{IN}}{n_{TR1} + n_{TR2}}. \quad (14)$$

From equations (9), (12), and (14), it can be noted that the proposed converter has three resonant points while doubling the output voltage, when V_{OUT} is $V_{IN}/(n_{TR1} + n_{TR2})$, $V_{IN}/(0.5n_{TR1} + n_{TR2})$, and $2V_{IN}/(n_{TR1} + n_{TR2})$. This means that the resonant current waveform of the proposed converter is inherently close to the sinusoidal waveform over the wide range of the output voltage. Accordingly, it can be inferred that the proposed converter will maintain high efficiency.

B. OPERATION IN PWM REGION

In this section the operation in PWM region is discussed, where the resonant current is not sinusoidal. In order to maximize the accuracy of the analysis, we are going to provide the time domain analysis of the proposed converter. The proposed converter operates based on the resonance between L_R and C_R. Here we define characteristics impedance $Z = \sqrt{L_R/C_R}$ and resonant frequency $\omega = 1/\sqrt{L_R C_R}$ for the following sections. It is assumed that L_M is large enough to approximate that L_M is open.

1) PWM1 REGION ($0.5 \le D_{SR1} \le 1$, $D_{SR2} = 0.5$)

Fig. 7 and Fig. 8 present the operation of the proposed applied to SR_1, and SR_2 still operates as synchronous rectifier. So, $D_{SR1} > 0.5$ and $D_{SR2} = 0.5$ with $F_S = F_R$. The boosting duty

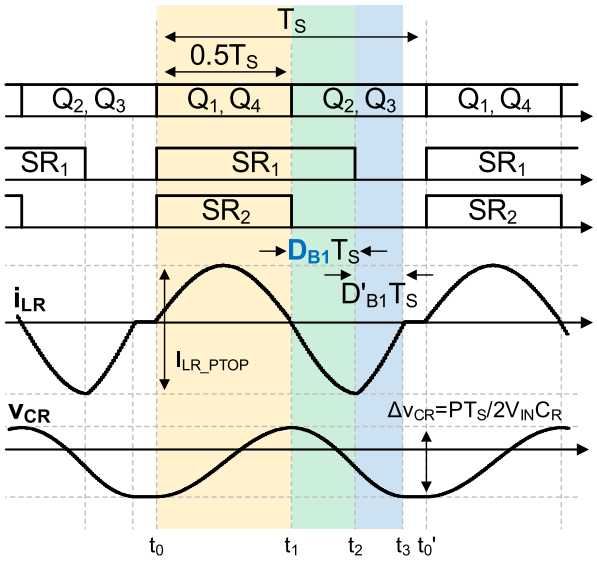

FIGURE 7. Key waveforms of the proposed converter in PWM1 region (0.5 < D_{SR1} < 1).

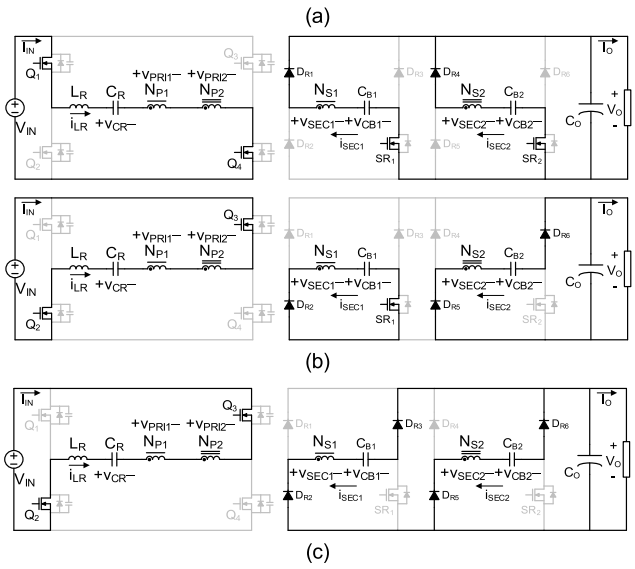

FIGURE 8. Current paths in PWM1 region (0.5 < D_{SR1} < 1) during (a) t_0~t_1, (b) t_1~t_2, (c) t_2~t_3.

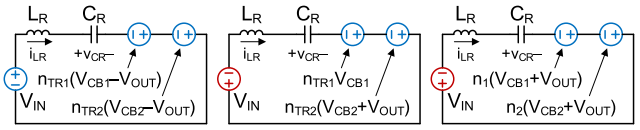

FIGURE 9. Equivalent resonant circuits in PWM1 region (0.5 < D_{SR1} < 1) during (a) t_0~t_1, (b) t_1~t_2, (c) t_2~t_3.

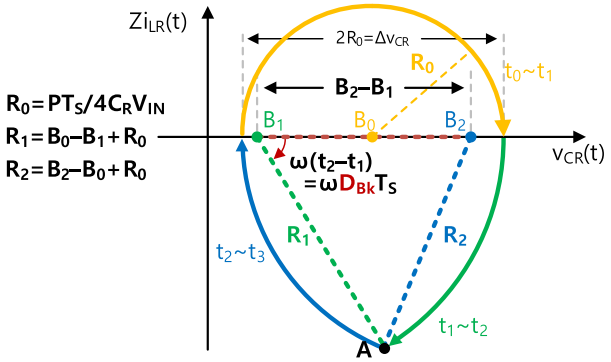

FIGURE 10. State plane in PWM k region (k = 1 or 2).

ratio applied to SR_1 in PWM1 region is defined as $D_{B1} = D_{SR1} - 0.5$.

Fig. 9 presents equivalent resonant circuits during t_0~t_1, t_1~t_2, and t_2~t_3, reflected to primary side. Analyzing three equivalent circuits allows us to find the required D_{SR1} at a specific operating point. During t_3~t_0', the resonant current maintains zero and voltage across resonant capacitor remains unchanged.

Q_1 and Q_4 are turned on at t_0. At t_0, $i_{LR} = 0$. Q_1 and Q_4 are turned on. The resonance between L_R and C_R begins. Duration of t_0~t_1 is $0.5T_S$. i_{LR} waveform becomes positive half cycle of sine wave. Input current of the converter flows through C_R, so $\Delta v_{CR} = I_{IN}T_S/2C_R = PT_S/4C_RV_{IN}$ where P, V_{IN}, and I_{IN} present operating power, input voltage, and input current of the converter respectively. State equations during t_0~t_1 can be obtained from Fig. 9(a) as follows:

$$Zi_{LR}(t - t_0) = A_0 \sin(\omega t), \tag{15}$$

$$v_{CR}(t - t_0) - v_{CR}(t_0) = A_0 [1 - \cos(\omega t)], \tag{16}$$

$$[v_{CR}(t - t_0) - B_0]^2 + [Zi_{LR(t-t_0)}]^2 = A_0^2 = R_0^2, \tag{17}$$

where

$$A_0 = V_{IN} + n_1V_{CB1} + n_2V_{CB2}(n_1 + n_2)V_{OUT} - v_{CR}(t_0) \tag{18}$$

$$B_0 = V_{IN} + n_1V_{CB1} + n_2V_{CB2} - (n_1 + n_2)V_{OUT} \tag{19}$$

$$R_0 = \Delta v_{CR}/2 = PT_S/4C_RV_{IN}. \tag{20}$$

It can be noted that the state equation (17) forms a circle C_0 located at the center (B_0, 0) as shown in Fig. 10. At t_1, i_{LR} becomes zero again and Q_1 and Q_4 are turned off.

Q_2 and Q_3 are turned on at t_1. At t_1, $i_{LR} = 0$. Q_2 and Q_3 are turned on. i_{LR} becomes negative. Q_{SR1} signal is extended to provide boosting period $D_{B1}T_S$. The resonant current is boosted quickly through TR_1 during this period. It should be noted that the boosted resonant current is still being delivered to the output capacitor through TR_2, D_{R5}, and D_{R6}, because SR_2 is turned off. On the other hand, the resonant current is not delivered to the output capacitor through TR_1 because SR_1 is still turned on. State equations during t_1~t_2 can be

obtained from Fig. 9(b) as follows:

$$Zi_{LR}(t-t_1) = A_1\sin(\omega t), \tag{21}$$

$$v_{CR}(t-t_1) - v_{CR}(t_1) = A_1[1-\cos(\omega t)], \tag{22}$$

$$[v_{CR}(t-t_1) - B_1]^2 + [Zi_{LR}(t-t_1)]^2 = R_1^2, \tag{23}$$

where

$$A_1 = -V_{IN} + n_1V_{CB1} + n_2V_{CB2} + n_2V_{OUT} - v_{CR}(t_1), \tag{24}$$

$$B_1 = -V_{IN} + n_1V_{CB1} + n_2V_{CB2} + n_2V_{OUT}, \tag{25}$$

The state equation (23) forms a circle C_1 located at the center $(B_1, 0)$ as shown in Fig. 10. At t_2, SR_1 is turned off. The radius $R_1 = B_0B_1 + R_0$.

SR_2 is turned off at t_2. The boosted resonant current is delivered to the output capacitor through both TR_1 and TR_2. i_{LR} decreases and the state equations during $t_2 \sim t_3$ can be obtained from Fig. 9(c) as follows:

$$Zi_{LR}(t-t_2) = A_2\sin(\omega t) + Zi_{LR}(t_2)\cos(\omega t), \tag{26}$$

$$v_{CR}(t-t_2) - v_{CR}(t_2) = A_2[1-\cos(\omega t)] + Zi_{LR}(t_2)\sin(\omega t), \tag{27}$$

$$[v_{CR}(t-t_2) - B_2]^2 + [Zi_{LR}(t-t_2)]^2 = R_2^2, \tag{28}$$

where

$$A_2 = -V_{IN} + n_1V_{CB1} + n_2V_{CB2} + (n_1+n_2)V_{OUT} - v_{CR}(t_2), \tag{29}$$

$$B_2 = -V_{IN} + n_1V_{CB1} + n_2V_{CB2} + (n_1+n_2)V_{OUT}, \tag{30}$$

$$R_2 = B_2 - B_0 + R_0. \tag{31}$$

The state equation (28) forms a circle C_2 located at the center $(B_2, 0)$ as shown in Fig. 10. At t_3, i_{LR} becomes zero again and the converter is in the idle state till the next switching period.

2) PWM2 REGION ($D_{SR1} = 1$, $0.5 \le D_{SR2} \le 1$)

SR_1 is fully turned on when $D_{SR1} = 1$, and the proposed converter meets the second resonant point. The secondary side rectifier having SR_1 becomes voltage doubler rectifier, and v_{CB1} becomes $0.5V_O$. Now D_{SR2} increases as output voltage needs to be increased, and the proposed converter operates in PWM2 region. $D_{SR1} = 1$ and $D_{SR2} > 0.5$ with $F_S = F_R$. The boosting duty ratio applied to SR_2 in PWM2 region is defined as $D_{B2} = D_{SR2} - 0.5$. Fig. 11, 12, and 13 present key waveforms, current paths, and resonant circuits of the proposed converter in PWM2 region respectively. It can be noted that the operation of the proposed converter in PWM2 region is similar with that of PWM1 region, having the same equations and state planes for $Zi_{LR}(t)$ and $v_{CR}(t)$ except for the coefficients A_0, A_1, A_2, B_0, B_1, and B_2. We can just summarize the coefficients as follows:

$$A_0 = V_{IN} + n_1V_{CB1} + n_2V_{CB2}(n_1+n_2)V_{OUT} - v_{CR}(t_0), \tag{32}$$

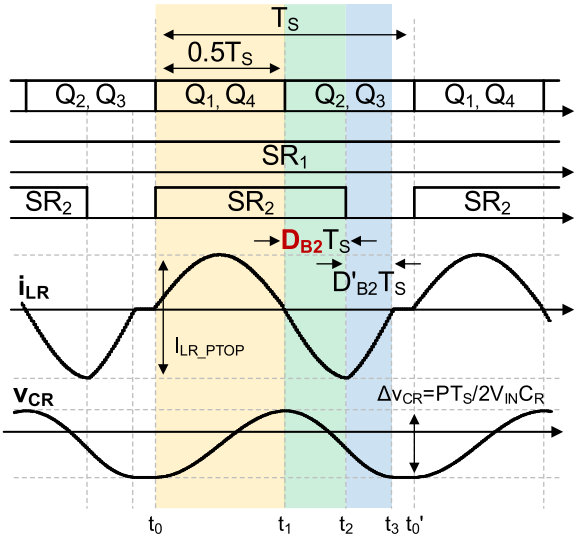

FIGURE 11. Key waveforms of the proposed converter in PWM 2 region ($D_{SR1} = 1$, $0.5 < D_{SR2} < 1$).

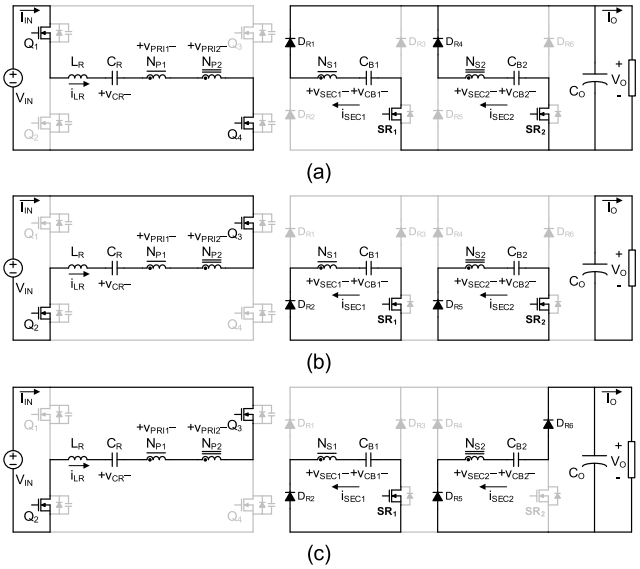

FIGURE 12. Current paths in PWM2 region ($D_{SR1} = 1$, $0.5 < D_{SR2} < 1$) during (a) $t_0 \sim t_1$, (b) $t_1 \sim t_2$, (c) $t_2 \sim t_3$.

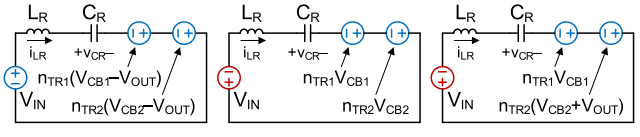

FIGURE 13. Equivalent resonant circuits in PWM2 region ($D_{SR1} = 1$, $0.5 < D_{SR2} < 1$) during (a) $t_0 \sim t_1$, (b) $t_1 \sim t_2$, (c) $t_2 \sim t_3$.

$$B_0 = V_{IN} + n_1V_{CB1} + n_2V_{CB2} - (n_1+n_2)V_{OUT}, \tag{33}$$

$$A_1 = -V_{IN} + n_1V_{CB1} + n_2V_{CB2} - v_{CR}(t_1), \tag{34}$$

$$B_1 = -V_{IN} + n_1V_{CB1} + n_2V_{CB2}, \tag{35}$$

$$A_2 = -V_{IN} + n_1 V_{CB1} + n_2 V_{CB2} + n_2 V_{OUT} - v_{CR}(t_2), \quad (36)$$

$$B_2 = -V_{IN} + n_1 V_{CB1} + n_2 V_{CB2} + n_2 V_{OUT}, \quad (37)$$

C. REQUIRED BOOSTING DUTY RATIO

Required boosting duty ratio in PWM k region (D_{Bk}, k = 1 or 2) can be presented by a single equation in both PWM1 and PWM2 regions, because both regions have identical state plane as shown in Fig. 10. D_{Bk} under a specific operating point can be obtained by applying the cosine law to the angle $A\mathbf{B_1}B_2$ in Fig. 10, given operating conditions (P, T_S, V_{IN}, V_{OUT}, L_R, C_R, n_{TR1}, n_{TR2}, and P) as follows:

$$R_2^2 = R_1^2 + (B_2 - B_1)^2 2R_1(B_2 - B_1)\cos(\omega D_{Bk} T_S). \quad (38)$$

Rearranging (28) leads to the following equation regarding D_{Bk}:

$$D_{Bk} = \frac{1}{2\pi} cos^{-1}\left[\frac{R_1^2 + (B_2 - B_1)^2 - R_2^2}{2R_1(B_2 - B_1)}\right]. \quad (39)$$

The only difference between PWM 1 and 2 regions is the coefficient values R_1, R_2, B_1, and B_2. From (39) and previous analysis, it can be noted that the only unknown variables V_{CB1} and V_{CB2} are cancelled out in (B_2–B_1) so that all variables for D_{Bk} calculation are known, related to the operating condition of the proposed converter. Additionally, if we define the time duration t_3–t_2 as $D'_{Bk}T_S$, D'_{Bk} can be obtained by applying the cosine law to the angle $A\mathbf{B_2}B_1$ as follows:

$$D'_{Bk} = \frac{1}{2\pi} cos^{-1}\left[\frac{R_2^2 + (B_2 - B_1)^2 - R_1^2}{2R_2(B_2 - B_1)}\right]. \quad (40)$$

D. VOLTAGE ACROSS THE BLOCKING CAPACITORS

As the output voltage increases by twice, it can be intuitively seen that the voltage across the blocking capacitors V_{CB1} and V_{CB2} increase from zero to $V_O/2$. This is because the secondary side rectifier morphs from full bridge rectifier to voltage doubler as V_O increases. V_{CB1} and V_{CB2} in PWM 1 region can be obtained by applying the volt-sec balance to the secondary side of two transformers as follows:

$$V_{CB1} = \frac{0.5 - D'_{B1}}{0.5 + D_{B1} + D'_{B1}} V_O, \quad (41)$$

$$V_{CB2} = \frac{0.5 - (D_{B1} + D'_{B1})}{0.5 + D_{B1} + D'_{B1}} V_O. \quad (42)$$

In the same manner, V_{CB1} and V_{CB2} in PWM 2 region can be obtained by applying the volt-sec balance to the secondary side of two transformers as follows:

$$V_{CB1} = \frac{0.5}{0.5 + D_{B2} + D'_{B2}} V_O, \quad (43)$$

$$V_{CB2} = \frac{0.5 - D'_{B2}}{0.5 + D_{B2} + D'_{B2}} V_O. \quad (44)$$

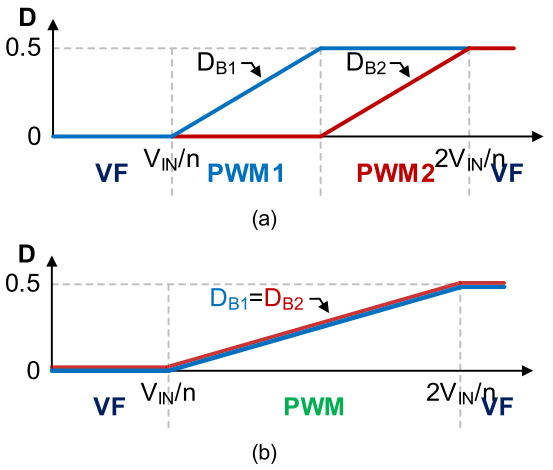

FIGURE 14. Control concept comparison (a) proposed sequential PWM and (b) PWM without sequence.

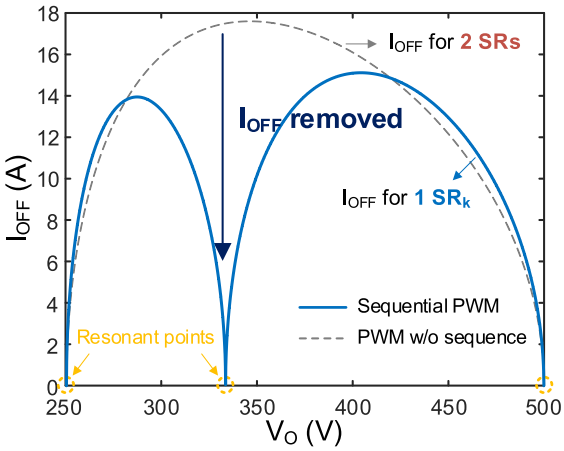

FIGURE 15. I_{OFF} comparison in PWM regions at full load condition.

Finally, we have all the expressions for the variables required to obtain explicit form of $i_{LR}(t)$ and $v_{CR}(t)$ during a switching period. Based on the equations, design and comparative analysis will be provided in the following section.

IV. DESIGN AND COMPARATIVE ANALYSIS

In order to discuss effectiveness of the sequential PWM with the proposed converter, comparison with PWM without sequence will be provided in this section. Fig. 15 presents control concept of two methods. The proposed "sequential PWM" increases D_{SR1} first and then increases D_{SR2} when the output voltage increases from V_{IN}/n to $2V_{IN}/n$, whereas "PWM without sequence" increases D_{SR1} and D_{SR2} simultaneously. Since the analysis for PWM without sequence is very similar to that of the proposed control, detailed equations are not shown.

Prototype converter has been designed for 3.3 kW/500∼150 V/11 A EV on-board charger (OBC) with 400 V input voltage. Battery charging V-I curve is shown in Fig. 1. The

input voltage is 400 V.F_S and F_R are selected to be 100 kHz as an example.

A. TURNS RATIO OF THE TRANSFORMER

The proposed converter provides doubled output voltage without varying the switching frequency according to Fig. 14. When the proposed converter provides 500 V output voltage at the third resonant point, the proposed converter can decrease the output voltage down to 250 V at the first resonant point, without switching frequency control. In EV OBC applications, 500 V to 250 V range is much wider than the voltage range where the efficiency is critical, because users usually manage the battery voltage in a much narrower range. Therefore, it is reasonable to let PWM regions cover 500∼250 V range and focus on maximizing efficiency in PWM regions. According to (2), the effective turns ratio n can be obtained as follows:

$$n = n_{TR1} + n_{TR2} = \frac{V_{IN}}{V_O} = \frac{400}{250} = 1.6, \tag{45}$$

For simplicity, n_{TR1} and n_{TR2} are selected to be 0.8 each.

B. RESONANT TANK

The proposed converter does not rely on the circulating magnetizing current of the transformer to achieve a boosting gain. Therefore, selection of the resonant tank values L_R and C_R does not rely on the gain range. We may minimize L_R in order to have a smaller size of L_R. However, there is a tradeoff between L_R size and loss. According to previous researches regarding PWM resonant converters [4], [5], [6], [7], [8], [9], [10], smaller L_R results in a larger turnoff current in the boosting switch and a larger L_R current swing, resulting in larger turnoff switching loss and also larger L_R loss. Considering the tradeoff, L_R is selected to be 38 μH as an example.

C. TURNOFF CURRENT COMPARISON

From the state plane analysis in Fig. 10, turnoff current of a boosting switch I_{OFF} in PWM k region can be obtained as follows:

$$I_{OFF} = \frac{n_{TRk} R_1 \sin(\omega D_{Bk} T_S)}{Z}, \tag{46}$$

Fig. 15 presents I_{OFF} comparison in PWM regions according to V_O at full load condition. With the proposed sequential PWM, I_{OFF} becomes zero three times as V_O increases from 250 to 500 V because it has three resonant points in V_O range. On the other hand, PWM without sequence has only two resonant points resulting in a high peak value of I_{OFF} around 330 V, where the proposed method achieves the second resonant point. Furthermore, the proposed method has only single SR switch suffering from the turnoff switching loss in each PWM region. In PWM k region, only SR_k has turnoff switching loss. On the other hand, PWM without sequence has both SR switches producing turnoff switching loss with larger I_{OFF}. Accordingly, the proposed sequential PWM can reduce the turnoff switching loss dramatically in the entire PWM regions.

TABLE 1. Parts list for prototype converter (Fig. 3).

Symbol	Part	Specification
TR_1	Transformer 1	L_{M1}=103.3μH, L_{LKG1}=2.2μH PQ4040 core N_{P1}:N_{S1}=21:27 (0.1Φ*200 litz wires)
TR_2	Transformer 2	L_{M2}=102.8μH, L_{LKG2}=2.3μH PQ4040 core N_{P2}:N_{S2}=21:27 (0.1Φ*200 litz wires)
L_R	Resonant inductor	L_R=32.2μH PQ4040 core 23 turns, 0.1Φ*400 litz wire
C_R	Resonant capacitor	74nF film capacitors (F_R~100 kHz)
$C_{B1,2}$	Blocking capacitors	1μF film capacitors
Q_{1-4} $SR_{1,2}$ D_{R1-6}	Main and rectifier switches	NTH4L020N120SC1 12 EA (20 mΩ SiC MOSFET)

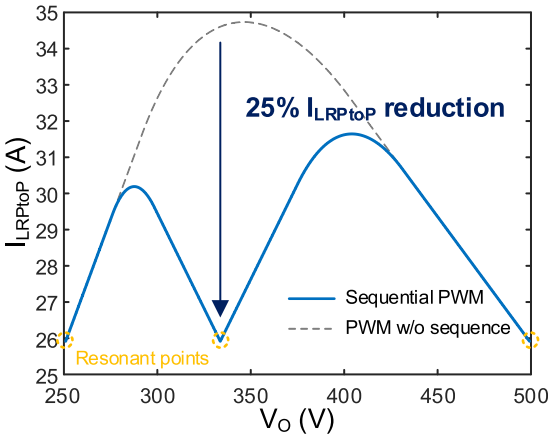

FIGURE 16. I_{LRPtoP} comparison in PWM regions at full load condition.

D. PEAK-TO-PEAK VALUE OF i_{LR} COMPARISON

Another important variable in PWM resonant converter is peak-to-peak value of the resonant current I_{LRPtoP}. This is because I_{LR_PTOP} is directly proportional to the maximum flux swing of L_R. Utilizing $i_{LR}(t)$ from the previous chapter, Fig. 16 presents I_{LRPtoP} comparison in PWM regions according to V_O at full load condition. It can be also seen that the proposed method reduces the flux swing of L_R by up to 25 % having three resonant points in the operating voltage range.

V. EXPERIMENTAL RESULTS

Prototype converter has been built to verify the effectiveness of the proposed converter with sequential boosting PWM control. Table 1 presents parts list for the prototype converter. Synchronous rectifiers are used instead of diodes for $D_{R1\sim6}$. Fig. 17 presents V_O versus total boosting duty ratio $D_B(=D_{B1} + D_{B2})$ in different loading conditions. It can

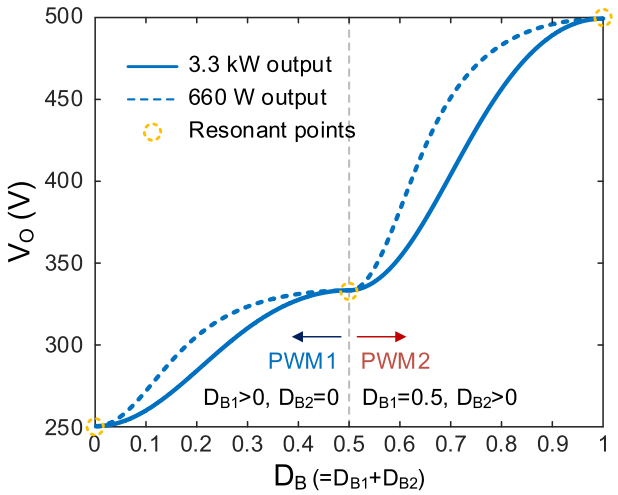

FIGURE 17. V_O versus D_B(=D_{B1} + D_{B2}) in 3.3 kW and 660 W conditions.

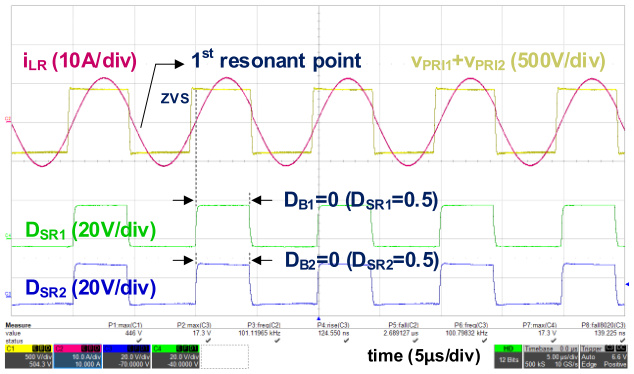

FIGURE 18. Key waveforms of prototype at 255 V/11 A output (D_B = 0).

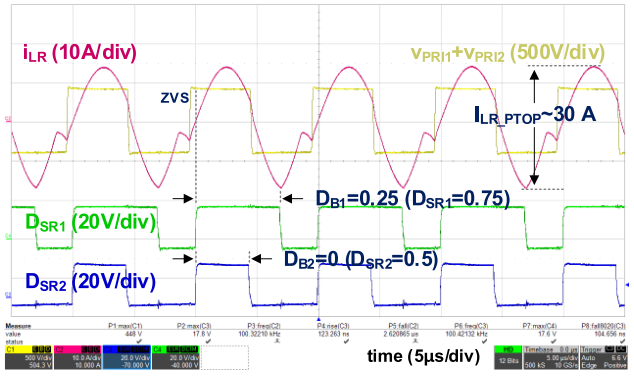

FIGURE 19. Key waveforms of prototype at 303 V/11 A output (D_B = 0.25).

be noted that the proposed converter has steadily increasing V_O with respect to D_B, allowing us to control the proposed converter.

Fig. 18. presents the key waveforms of the prototype at 254 V/11 A output condition. The proposed converter operates at the first resonant point, having a sinusoidal resonant current waveform. $D_B = D_{B1} = D_{B2} = 0$.

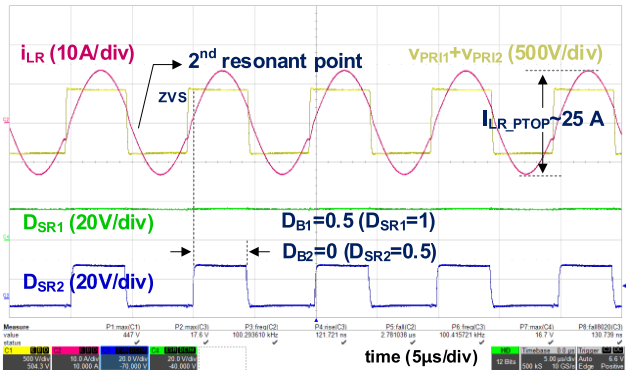

FIGURE 20. Key waveforms of prototype at 340 V/3.3 kW output (D_B = 0.5).

TABLE 2. Comparison with previous prior arts for 3.3 kW EV chargers.

Works	Topology	Control	Efficiency @ 3.3 kW
[12]	Series Resonant	PWM–boost	98.1~97.4 %
[16]	LLC	PWM+PFM	96.3~96.9 %
[20]	Series Resonant	PWM morphing	98.5~97.9 %
Proposed	**Series Resonant**	**Sequential PWM–boost**	**98.8~98.3 %**

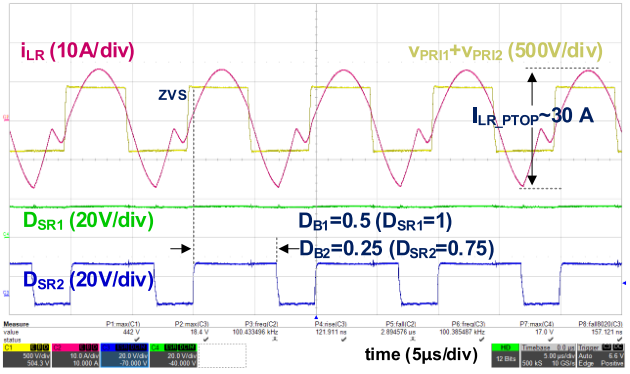

FIGURE 21. Key waveforms of prototype at 375 V/3.3 kW output (D_B = 0.75).

Fig. 19 presents the key waveforms of the prototype at 303 V/11 A output condition. The proposed converter increases D_B to 0.25 to obtain a boosted gain. D_{B1} is increased for a larger D_B. The proposed converter operates in PWM1 region.

Fig. 20 presents the key waveforms of the prototype at 340 V/3.3 kW output condition. D_B is increased to 0.5 and SR_1 is fully turned on. The proposed converter operates at the second resonant point, having a sinusoidal resonant current waveform again.

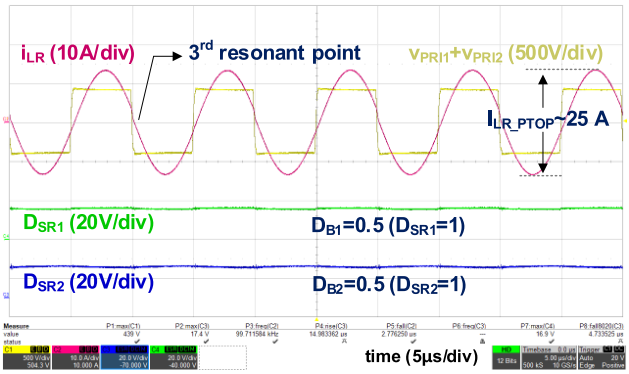

FIGURE 22. Key waveforms of prototype at 507 V/3.3 kW output ($D_B = 1$).

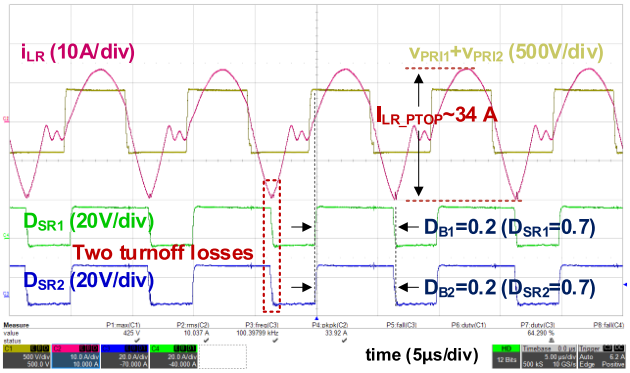

FIGURE 23. Key waveforms of prototype using "PWM w/o sequence" at 360 V/3.3 kW condition.

Fig. 21 presents the key waveforms of the prototype at 375 V/3.3 kW output condition. The proposed converter increases D_B to 0.75 to obtain a boosted gain. Now D_{B2} is increased for a larger D_B. The proposed converter operates in PWM2 region.

Fig. 22 presents the key waveforms of the prototype at 507 V/3.3 kW output condition. D_B is increased to 1 and both SR_1 and SR_2 are fully turned on. The proposed converter operates at the third resonant point, having a sinusoidal resonant current waveform again.

Fig. 23 presents the key waveforms of the prototype using PWM without sequence at 360 V/3.3 kW output condition. D_{B1} and D_{B2} are increased simultaneously to obtain a boosting gain. As analyzed in the previous chapter, the resonant current has much larger peak to peak value because PWM without sequence has only two resonant points in the operating voltage range. In order to reduce the peak to peak current, L_R needs to be increased, resulting in a larger size of L_R. Furthermore, it can be noted that both SR_1 and SR_2 are suffering a large switching turnoff loss at the secondary side.

Fig. 24 presents the efficiency of the prototype converter. Over 250∼500 V output voltage range, the proposed sequential PWM achieves 98.82 % peak and 98.25 % valley efficiency. By having three resonant points, the proposed method effectively limits efficiency drop. On the other hand, PWM

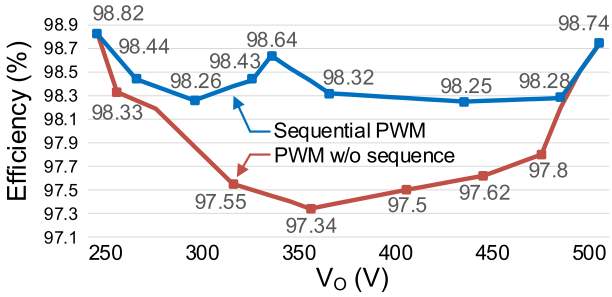

FIGURE 24. Measured efficiency of the prototype at full load conditions.

without sequence fails to maintain high efficiency due to a large L_R current swing and turnoff losses from two boosting switches. Prototype converter utilizes variable frequency control when the output voltage is lower than 250 V. The efficiency drops to 96.4 % and 93.7 % when the output voltage is 200 V and 150 V respectively, but the efficiency is not important in this region.

Table 2 presents comparison with the previous state-of-the-art technologies for 3.3 kW EV chargers. As shown in the table, it can be noted that the proposed converter improves efficiency in the maximum output power region compared to prior works, with the help of SIPO structure and sequential PWM technique.

VI. CONCLUSION

This paper proposed sequential PWM control for a resonant converter with series input parallel output transformer structure. Series input parallel output structure effectively achieves current sharing and reduced current stress at the output side, which is well in accordance with the recent requirements for higher charging power in EV charging applications. By adapting sequential PWM control, the proposed converter achieves multiple resonant points while doubling the output voltage. The efficiency drop is limited by placing more resonant points in the same output voltage range, compared to PWM without sequence. Both peak to peak current and switching turnoff loss have been significantly reduced. As a result, the proposed method maintains high-competitive efficiency with small size of the resonant inductor, which is desirable characteristic for EV charging applications.

REFERENCES

[1] F. C. Lee, Q. Li, and A. Nabih, "High frequency resonant converters: An overview on the magnetic design and control methods," *IEEE J. Emerg. Sel. Top. Power Electron.*, vol. 9, no. 1, pp. 11–23, Feb. 2021.

[2] F. Musavi, M. Cracium, D. S. Gautam, and W. Eberle, "Control strategies for wide output voltage range LLC resonant DC–DC converters in battery chargers," *IEEE Trans. Veh. Technol.*, vol. 63, no. 3, pp. 1117–1125, Mar. 2014.

[3] J. Deng, S. Li, S. Hu, C. C. Mi, and R. Ma, "Design methodology of LLC resonant converters for electric vehicle battery chargers," *IEEE Trans. Veh. Technol.*, vol. 63, no. 4, pp. 1581–1592, May 2014.

[4] F. Musavi, M. Craciun, D. S. Gautam, W. Eberle, and W. G. Dunford, "An LLC resonant DC–DC converter for wide output voltage range battery charging applications," *IEEE Trans. Power Electron.*, vol. 28, no. 12, pp. 5437–5445, Dec. 2013.

[5] C.-O. Yeon, J.-W. Kim, M.-H. Park, I.-O. Lee, and G.-W. Moon, "Improving the light-load regulation capability of LLC series resonant converter using impedance analysis," *IEEE Trans. Power Electron.*, vol. 32, no. 9, pp. 7056–7067, Sep. 2017.
[6] J.-W. Kim, J.-P. Moon, and G.-W. Moon, "Duty-ratio-control-aided LLC converter for current balancing of two-channel LED driver," *IEEE Trans. Ind. Electron.*, vol. 64, no. 2, pp. 1178–1184, Feb. 2017.
[7] J.-W. Kim, M.-H. Park, B.-H. Lee, and J.-S. Lai, "Analysis and design of *LLC* converter considering output voltage regulation under no-load condition," *IEEE Trans. Power Electron.*, vol. 35, no. 1, pp. 522–534, Jan. 2020.
[8] A. Mustafa and S. Mekhilef, "Dual phase LLC resonant converter with variable frequency zero circulating current phase-shift modulation for wide input voltage range applications," *IEEE Trans. Power Electron.*, vol. 36, no. 3, pp. 2793–2807, Mar. 2021.
[9] J.-W. Kim, M.-H. Park, J.-K. Han, M. Lee, and J.-S. Lai, "PWM resonant converter with asymmetric modulation for ZVS active voltage doubler rectifier and forced half resonance in PV application," *IEEE Trans. Power Electron.*, vol. 35, no. 1, pp. 508–521, Jan. 2020.
[10] X. Zhao, C.-W. Chen, and J.-S. Lai, "A high-efficiency active-boost-rectifier-based converter with a novel double-pulse duty cycle modulation for PV to DC microgrid applications," *IEEE Trans. Power Electron.*, vol. 34, no. 8, pp. 7462–7473, Aug. 2019.
[11] J.-W. Kim, M. Lee, and J.-S. Lai, "Efficient *LLC* resonant converter with a simple hold-up time compensation in voltage doubler rectifier," *IEEE J. Emerg. Sel. Topics Power Electron.*, vol. 7, no. 2, pp. 843–850, Jun. 2019.
[12] G. Liu, Y. Jang, M. M. Jovanovi, and J. Q. Zhang, "Implementation of a 3.3-kW DC–DC converter for EV on-board charger employing the series-resonant converter with reduced-frequency-range control," *IEEE Trans. Power Electron.*, vol. 32, no. 6, pp. 4168–4184, Jun. 2017.
[13] T. LaBella, W. Yu, J.-S. Lai, M. Senesky, and D. Anderson, "A bidirectional-switch-based wide-input range high-efficiency isolated resonant converter for photovoltaic applications," *IEEE Trans. Power Electron.*, vol. 29, no. 7, pp. 3473–3484, Jul. 2014.
[14] X. Zhao, L. Zhang, R. Born, and J.-S. Lai, "A high-efficiency hybrid resonant converter with wide-input regulation for photovoltaic applications," *IEEE Trans. Ind. Electron.*, vol. 64, no. 5, pp. 3684–3695, May 2017.
[15] J.-W. Kim and G.-W. Moon, "A new LLC series resonant converter with a narrow switching frequency variation and reduced conduction losses," *IEEE Trans. Power Electron.*, vol. 29, no. 8, pp. 4278–4287, Aug. 2014.
[16] X. Tang, Y. Xing, H. Wu, and J. Zhao, "An improved *LLC* resonant converter with reconfigurable hybrid voltage multiplier and PWM-plus-PFM hybrid control for wide output range applications," *IEEE Trans. Power Electron.*, vol. 35, no. 1, pp. 185–197, Jan. 2020.
[17] D. Shu and H. Wang, "An ultrawide output range *LLC* resonant converter based on adjustable turns ratio transformer and reconfigurable bridge," *IEEE Trans. Ind. Electron.*, vol. 68, no. 8, pp. 7115–7124, Aug. 2021.
[18] M. M. Jovanović and B. T. Irving, "On-the-fly topology-morphing control-efficiency optimization method for *LLC* resonant converters operating in wide input- and/or output-voltage range," *IEEE Trans. Power Electron.*, vol. 31, no. 3, pp. 2596–2608, Mar. 2016.
[19] L. A. D. Ta, N. D. Dao, and D.-C. Lee, "High-efficiency hybrid LLC resonant converter for on-board chargers of plug-in electric vehicles," *IEEE Trans. Power Electron.*, vol. 35, no. 8, pp. 8324–8334, Aug. 2020.
[20] J.-W. Kim and P. Barbosa, "PWM-controlled series resonant converter for universal electric vehicle charger," *IEEE Trans. Power Electron.*, vol. 36, no. 12, pp. 13578–13588, Dec. 2021.
[21] S. Mukherjee, J. M. Ruiz, and P. Barbosa, "A high power density wide range DC–DC converter for universal electric vehicle charging," *IEEE Trans. Power Electron.*, vol. 38, no. 2, pp. 1998–2012, Feb. 2023.
[22] S. Mukherjee, V. Yousefzadeh, A. Sepahvand, M. Doshi, and D. Maksimovic, "High-frequency wide-range resonant converter operating as an automotive LED driver," *IEEE J. Emerg. Sel. Topics Power Electron.*, vol. 9, no. 5, pp. 5781–5794, Oct. 2021.
[23] C. Zhang, P. Barbosa, Z. Shen, and R. Wang, "A novel three-level phase-shift modulation for serial half bridge LLC resonant converter," in *Proc. IEEE Appl. Power Electron. Conf. Expo. (APEC)*, Jun. 2021, pp. 355–362.
[24] H. Xu, Z. Yin, Y. Zhao, and Y. Huang, "Accurate design of high-efficiency LLC resonant converter with wide output voltage," *IEEE Access*, vol. 5, pp. 26653–26665, 2017.

JONG-WOO KIM (Member, IEEE) received the B.S., M.S., and Ph.D. degrees in electrical engineering from the Korea Advanced Institute of Science and Technology (KAIST), Daejeon, South Korea, in 2010, 2012, and 2016, respectively.

From 2016 to 2019, he was a Research Assistant Professor and a Postdoctoral Researcher with Virginia Tech, Blacksburg, VA, USA. From 2019 to 2021, he was a member of Research and Development Staff with the M. Jovanović Power Electronics Laboratory, Delta Products Corporation, Research Triangle Park, NC, USA. From 2021 to 2022, he was a Power Hardware Engineer with Meta Platforms (formerly Facebook Inc.), Menlo Park, CA, USA. Since 2022, he has been an Assistant Professor with the Department of Electrical and Electronics Engineering, Konkuk University, Seoul, South Korea. He has authored/coauthored 23 journal articles and more than 20 technical papers in conference proceedings. His research interests include high efficiency power converters, high power density design with magnetic component integration, PCB winding, and wide bandgap devices, EMI noise reduction techniques, and analog/digital control for datacenter power and electric vehicle charging infrastructure.

DOHONG LEE (Student Member, IEEE) was born in Busan, South Korea, in 1993. He received the B.S. degree in electrical engineering from Konkuk University, Seoul, South Korea, in 2018, where he is currently pursuing the Ph.D. degree in power electronics. His current research interests include on-board charger and multilevel converters for the microgrid systems.

YOUNGHOON CHO (Senior Member, IEEE) was born in Seoul, South Korea, in 1980. He received the B.S. degree in electrical engineering from Konkuk University, Seoul, in 2002, the M.S. degree in electrical engineering from Seoul National University, Seoul, in 2004, and the Ph.D. degree in electrical engineering from Virginia Polytechnic Institute and State University, Blacksburg, VA, USA, in 2012. From 2004 to 2009, he was an Assistant Research Engineer with Hyundai MOBIS Research and Development Center, Yongin-si, South Korea. Since 2013, he has been with the Department of Electrical and Electronics Engineering, Konkuk University, where he is currently a Professor. His current research interests include digital control techniques for the power electronic converters in vehicle and grid applications, multilevel converters, and high-performance motor drives.